Electronic Supplementary Material (ESI) for Journal of Materials Chemistry A.

Supporting Information

Nanoporous PdIr alloy for High-Efficiency and Durable Water Splitting in Acidic Media

Jinyue Shi[a‡], Cheng-wei Kao[b‡], Jiao Lan[a], Jang Kang[a], Ming Peng[a], Min Luo[c*], Ying-Rui Lu[b*], Shiguo Zhang[a*] and Yongwen Tan[a*]

[a]College of Materials Science and Engineering, Hunan University, Changsha, Hunan 410082, China.

[b]National Synchrotron Radiation Research Center, Hsinchu 300, Taiwan.

[c]Shanghai Technical Institute of Electronics & Information, Shanghai 201411, China.

‡ These authors contributed equally to the work.

E-mail: lu.yr@nsrrc.org.tw (Ying-Rui), luomin@sspu.edu.cn (Min Luo), zhangsg@hnu.edu.cn (Shiguo Zhang), tanyw@hnu.edu.cn (Yongwen Tan)

Experimental methods

Synthesis of np-PdIr:

The $Ni_{97}Pd_{0.75}Ir_{2.25}$, $Ni_{97}Pd_{1.5}Ir_{1.5}$, $Ni_{97}Pd_{2.25}Ir_{0.75}$ alloy ingot as for the mother alloy was synthesized by arc melting in vacuum to fabricate $Ni_{97}Pd_{0.75}Ir_{2.25}$, $Ni_{97}Pd_{1.5}Ir_{1.5}$, $Ni_{97}Pd_{2.25}Ir_{0.75}$ ribbons by single-roller melt spinning at a rotation rate of 3500 rpm. Then, the np-$Ni_{30}Pd_{17.5}Ir_{52.5}$, np-$Ni_{30}Pd_{35}Ir_{35}$, np-$Ni_{30}Pd_{52.5}Ir_{17.5}$ was synthesized by electrochemical dealloying process at a voltage of 0.2 V versus Ag/AgCl/saturated KCl reference electrode for about 1000 s in 0.1 M HCl (Sinopharm Chemical ReagentCo., Ltd, AR, 36. 0%-38.0 %) to realize the corrosion of the most Ni component (**Figure S1**). The dealloying samples were cleaned by deionized water more than three times and dried in vacuum drying oven overnight. After then, 5 mg of np-NiPdIr powder was respectively dispersed in a solution containing 0.5 mL of ethanol (Greagent, AR, ≥99.7%) and 15 μL of Nafion solution (Adamas, RG, 5 wt%) by sonication for 1 h. After that, 30 μL of ink was dropped on a carbon paper and drying in the air for several hours. Subsequently, the self-activation process was conducted by performing repeated cyclic voltammetry (CV) scans (from the 10th cycle to the 500th cycle with the step of 50 cycles) between 0.0 V and 0.6 V versus RHE in 0.1 M HCl to gradually remove nickel species (**Figure S2**).[1] The above catalysts with different precursor-atomic-ratio were denoted as np-$Pd_{25}Ir_{75}$, np-$Pd_{50}Ir_{50}$, np-$Pd_{75}Ir_{25}$.

Structure and composition characterizations:

XRD patterns were taken by using a Rigaku MiniFlex X-ray diffraction. SEM experiments were conducted on Zeiss Sigma HD (Oxford EDS). HAADF-STEM

images, selected area electron diffraction (SAED) image, and EDX mappings were recorded on a JEM-ARM 200F. The chemical state of the samples was carried out using XPS on Thermo Scientific ESCALAB250Xi spectrometer with the monochromatic Al Kα. The Ir L_3-edge and Pd K-edge XAFS spectra were recorded at the Beamline No. 01C1 in Taiwan Light Source. Faradaic efficiency tests were based on the Gas Chromatograph (solution-1A).

Electrochemical measurements:

All electrochemical properties were evaluated by a three-electrode electrochemical system (CHI-760E) at room temperature.[2-5] The OER and HER properties were characterized in 0.5 M H_2SO_4 (Sinopharm Chemical ReagentCo., Ltd, 95.0 %-98.0 %) with a scan rate of 5 mV s^{-1}, and the overpotential for water oxidation was evaluated at 10 mA cm^{-2} current density. The distance between the working electrode and the reference electrode (Hg/Hg_2SO_4) was set at 1 cm, carbon rod as counter electrode. Overall water splitting is performed in a two-electrode system. One np-$Pd_{50}Ir_{50}$ (or Ir/C) electrode acts as the positive electrode for OER and the other np-$Pd_{50}Ir_{50}$ (or Pt/C) is used as the negative electrode for HER.

All the applied potentials were converted to the reversible hydrogen electrode (RHE) potential (E_{RHE}) as shown follow:

$$E_{RHE} = E_{exp} + E_{ref}^{0} + 0.0592\,V \times pH$$

Where E_{exp} is the experimental potential with relative to the reference electrode, *E0 ref* equals 0.656 V at 25 ℃ for the saturated Hg/Hg_2SO_4 reference electrode and *pH* is the hydrogen ion concentration of the electrolyte solution.

All of inks are prepared at room temperature. For the preparation of np-$Pd_{25}Ir_{75}$, np-$Pd_{50}Ir_{50}$, np-$Pd_{75}Ir_{25}$ inks, 5 mg of mixed catalysts were uniformly dispersed in 1 mL of ethanol solution containing 30 μL of 5 wt % Nafion solution through sonication for 1 h by ultrasonic cell grinder. The mixed catalyst is composed of 1 mg of np-$Pd_{100-x}Ir_x$ powder and 4 mg of Carbon powder. For the preparation of Ir/C and Pt/C inks, 5 mg of Ir/C or Pt/C were uniformly dispersed in 1 mL ethanol solution containing 30 μL of 5 wt % Nafion solution after sonication for 1 h by ultrasonic cell grinder. Subsequently, 40 μL of ink were dropped on a carbon paper with an area of 1 cm^2 and dried in the air. The loading values on carbon paper for np-$Pd_{25}Ir_{75}$, np-$Pd_{50}Ir_{50}$, np-$Pd_{75}Ir_{25}$, Ir/C, and Pt/C were 200.00 μg_{total} cm^{-2} (40 μg_{Ir+Pd} cm^{-2}, 31.96 μg_{Ir} cm^{-2}), 200.00 μg_{total} cm^{-2} (40 μg_{Ir+Pd} cm^{-2}, 26.36 μg_{Ir} cm^{-2}), 200.00 μg_{total} cm^{-2} (40 μg_{Ir+Pd} cm^{-2}, 17.21 μg_{Ir} cm^{-2}), 200.00 μg_{total} cm^{-2} (20.00 μg_{Ir} cm^{-2}), and 200.00 μg_{total} cm^{-2} (20.00 μg_{Pt} cm^{-2}), respectively.

Electrochemical impedance spectroscopy (EIS) was conducted at 1.5 V versus RHE with an amplitude of 5 mV over the $10^6 \sim 10^{-1}$ Hz frequency range using the former electrochemical workstation (CHI-760E). The obtained solution resistance (*Rs*) for each electrolyte with different values was used for 95% *iR* correction, while the Nyquist plot showed the OER kinetics of each sample.[6] The Faradaic efficiency tests used H-cells separated by a Nafion 117 membrane (electrochemical flow cells) to ensure the gas tightness[7]. Ar is passed in and out at the working electrode and reference electrode side.

Calculation of the electrochemical surface areas (ECSA):

The ECSA was determined by integrating the hydrogen underpotential deposition area (H_{UPD} method) from cyclic voltammetry (CV). The ECSA was calculated from the equation as follow[8]:

$$ECSA = \frac{Q}{mC}$$

The *C* is the H adsorption/desorption charge density on materials, the C values 210 μC cm^{-2} on Pt[9] while 218 μC cm^{-2} on Ir[10]. The *m* refers to the metal loading of Pt/Ir. The *Q* was calculated from integrating the H_{UPD} desorption:

$$Q = \frac{S_{peak}}{v}$$

The S_{peak} is obtained by integrating after subtracting the double-layer current density from ~0.05 to ~0.3 V (*vs* RHE). The *v* is the scan rate of 10 mV s^{-1}. The specific results were given in the **Table S1**.

Calculation of the mass activity and specific activity:

In order to evaluate the mass activities of np-$Pd_{25}Ir_{75}$, np-$Pd_{50}Ir_{50}$, np-$Pd_{75}Ir_{25}$, Ir/C, and Pt/C, the activity values were normalized to Ir loading for OER while Ir, Pd or Pt loading for HER. The current density at an overpotential of 270 mV (OER) or 50 mV (HER) were chosen to assess the mass activity. The final results about OER tests are as shown in the **Table S2**, while the ones about HER are given in the **Table S5**.

Mass activity (MA) was calculated as follow:

$$MA = \frac{j_{\eta = 270\ mV/\ 70\ mV}}{mass\ density_{Ir\ +\ Pd/Pt}}$$

Specific activity (SA) was calculated as follow:

$$SA = \frac{MA}{Electrochemical\ Surface\ area}$$

Notably, the *Surface area* was calculated by H_{UPD} desorption method.

Calculation of TOF for OER:

The turnover frequency (TOF) per active site in the catalysts was calculated using the formula[11]:

$$TOF(O_2/s) = \frac{\#total\ oxygen\ turnover\ per\ geometric\ area}{\#active\ sites\ per\ geometric\ area}$$

The total number of hydrogen turnovers was calculated from the current density according to:

$$\#\ total\ hydrogen\ turnovers = \left(\eta \times |j| \frac{mA}{cm^2}\right)$$

$$\left(\frac{1\ C\ s^{-1}}{1000mA}\right)\left(\frac{1\ mol\ e^{-1}}{96485\ C}\right)\left(\frac{1\ mol\ O_2}{4\ mol\ e^{-1}}\right)\left(\frac{6.023 \times 10^{23}\ O_2\ molecules}{1\ mol\ O_2}\right)$$

$$= 1.56 \times 10^{15} \frac{O_2/s}{cm^2} per \frac{mA}{cm^2} \eta \cdot |j|$$

where η is the Faradic efficiency at the potential of 1.50 V.

The number of active sites were calculated as the total number of surface sites from ECSA together with the unit cell of the np-$Pd_{50}Ir_{50}$ catalysts. The surface sites (atoms cm_{real}^{-2}) is estimated by using the method suggested by **Reference 12:**

$$\#surface\ sites = \left(\frac{4atoms\ /\ unit\ cell}{2.817Å^3\ /\ unit\ cell}\right)^{\frac{2}{3}} = 3.21 \times 10^{15}\ atoms\ cm_{real}^{-2}$$

$$A_{ECSA} = ECSA \times m_{Ir+Pd} = 137.61\ m^2\ g_{Ir+Pd}^{-1} \times 40\ \mu g = 55.04\ cm_{ECSA}^2$$

Hence, the TOFs of catalysts can be calculated according to:

$$TOF_{(\eta = 270mV)} = \frac{\#total\ oxygen\ turnover}{\#surface\ sites\ \times\ A_{ECSA}} = \frac{1.56 \times 10^{15} \times 91\% \times |-100|}{3.21 \times 10^{15} \times 55.04} = 0.80\ O_2\ s^{-1}$$

Calculation of TOF for HER:

The turnover frequency (TOF) per active site in the catalysts was calculated using the formula[13]:

$$TOF(H_2/s) = \frac{\#total\ hydrogen\ turnover\ per\ geometric\ area}{\#active\ sites\ per\ geometric\ area}$$

The total number of hydrogen turnovers was calculated from the current density according to:

$$\#\ total\ hydrogen\ turnovers = \left(\eta \cdot |j| \frac{mA}{cm^2}\right)\left(\frac{1\ C\ s^{-1}}{1000mA}\right)\left(\frac{1\ mol\ e^{-1}}{96485\ C}\right)\left(\frac{1\ mol\ H_2}{2\ mol\ e^{-1}}\right)\left(\frac{6.023 \times 10^{23}\ H_2\ molecules}{1\ mol\ H_2}\right)$$

$$= 3.12 \times 10^{15} \frac{H_2/s}{cm^2} per \frac{mA}{cm^2} \eta \cdot |j|$$

where η is the Faradic efficiency at the potential of -0.1 V. The numbers of surface sites in the np-$Pd_{50}Ir_{50}$ catalysts were calculated in the same way:

$$\#surface\ sites = \left(\frac{4atoms\ /\ unit\ cell}{2.817\text{Å}^3\ /\ unit\ cell}\right)^{\frac{2}{3}} = 3.21 \times 10^{15} sites\ per\ cm^2$$

Hence, the TOFs of catalysts can be calculated according to:

$$TOF_{(\eta = 0.1\ V)} = \frac{\#total\ oxygen\ turnover}{\#surface\ sites\ \times\ A_{ECSA}} = \frac{3.12 \times 10^{15} \times 98\% \times |-100|}{3.21 \times 10^{15} \times 55.04} = 1.73\ H_2\ s^{-1}$$

Calculation for Faradaic Efficiency (FE):

The FE test was based on Gas Chromatograph (GC) technique. The equation is as follows:

$$FE = \frac{Q_{H_2/O_2}}{Q_{total}} = \frac{x \times F \times n_{total} \times C_{H_2/O_2}}{I \times t}$$

Where x is the number of electron transfers for HER (x=2) and OER (x=4), F is the Faradaic constant, n_{total} is a theoretical value calculated by the corresponding current

(I) and reaction time (t), and the $C_{H2/O2}$ is related to the characteristic peak integration corresponding to the GC spectrum. The specific results were shown in the **Figure S11 (OER) and Figure S14 (HER).**

DFT calculations:

All of the computations were performed by means of spin-polarized DFT methods using the Vienna Ab initio Simulation Package (VASP).[14] The spin-polarized projector augmented wave (PAW) projectors and the Perdew-Burke-Ernzerhof (PBE) functional of generalized gradient approximation (GGA) is utilized to describe the electronic structures of given structure. The free energies of oxygen species are calculated on the dominant crystal surface of Ir(111) and Pd(111). In the same way, the free energies of hydrogen species are calculated on the dominant crystal surface of Ir(111) and Pd(111).

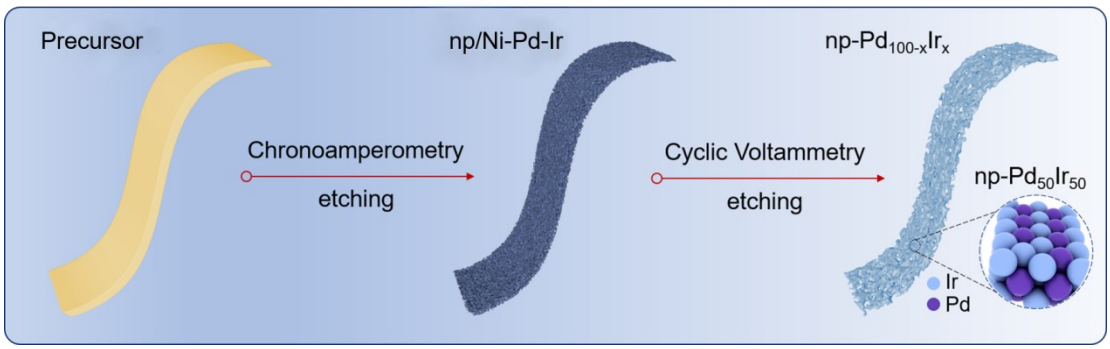

Figure S1. Chemical description of the fabrication process of nanoporous $Pd_{100-x}Ir_x$.

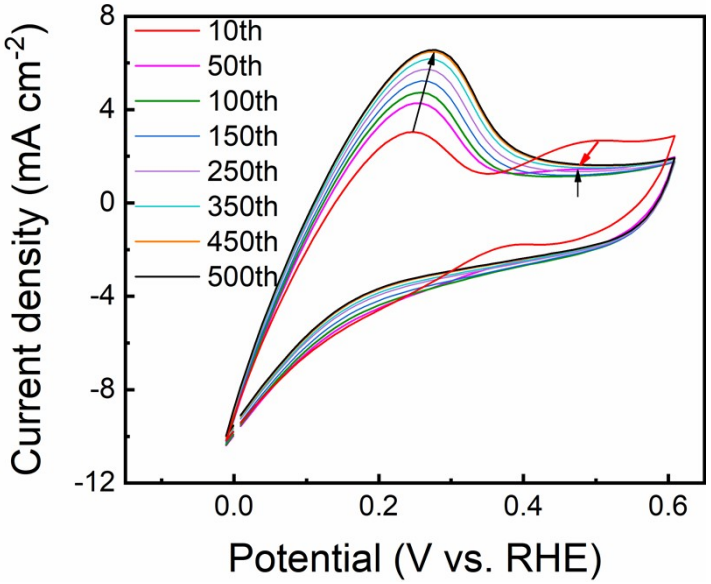

Figure S2. The CV curves of np-$Pd_{50}Ir_{50}$ in 0.1 M HCl with 50 mV s^{-1}.

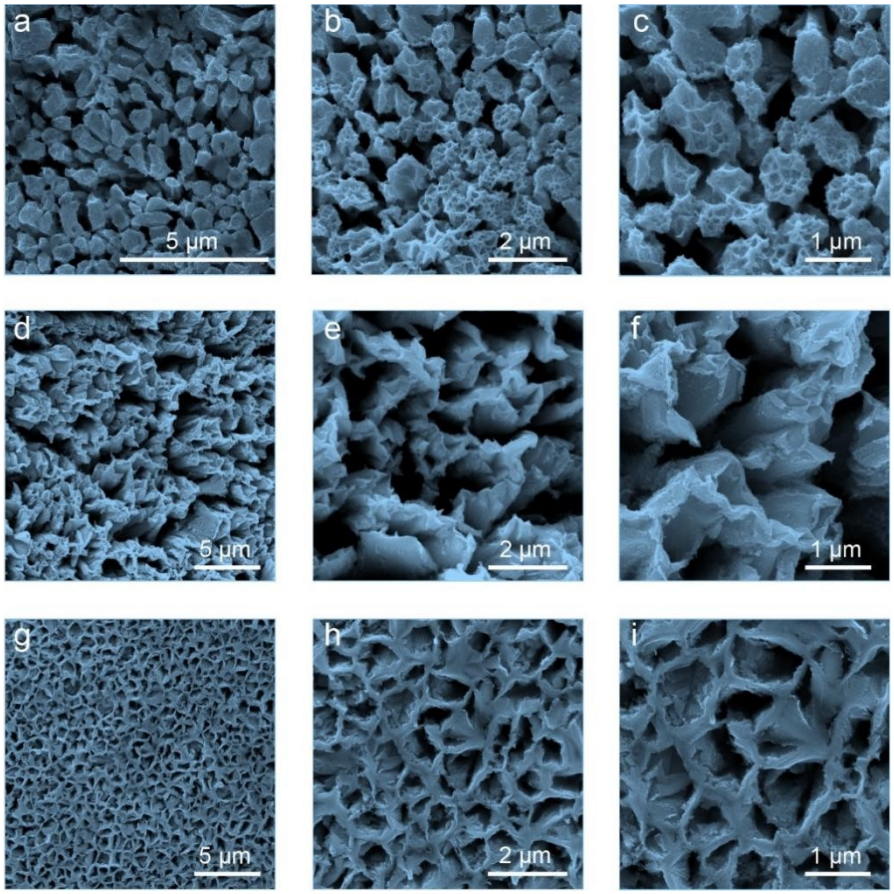

Figure S3. The SEM images of **(a-c)** np-$Pd_{25}Ir_{75}$, **(d-f)** 4np-$Pd_{50}Ir_{50}$, **(g-i)** np-$Pd_{75}Ir_{25}$.

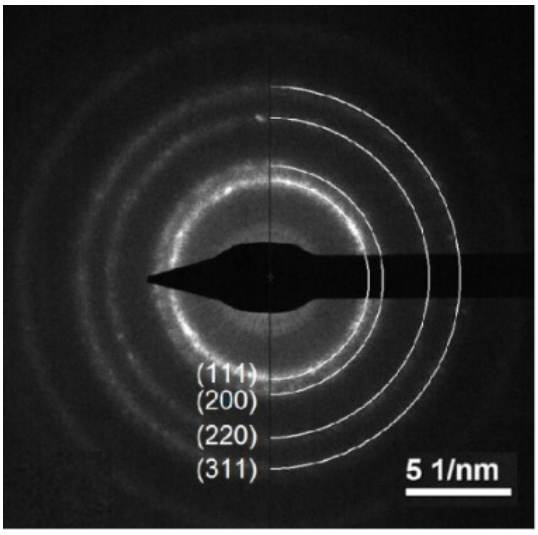

Figure S4. X-ray Polycrystalline electron diffraction pattern of np-$Pd_{50}Ir_{50}$.

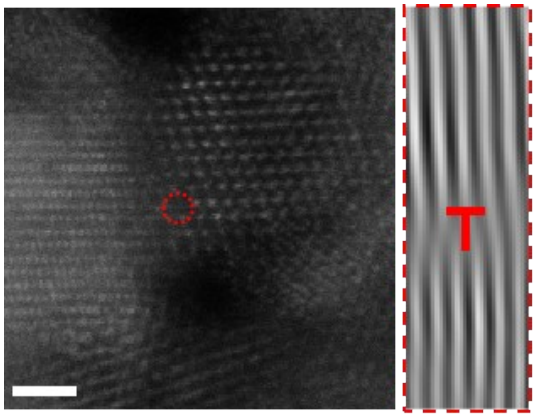

Figure S5. The HRTEM of np-$Pd_{50}Ir_{50}$.

The dotted line indicates that the lattice stripe in the red circle, showing some dislocation defects. Scale bar: 2 nm.

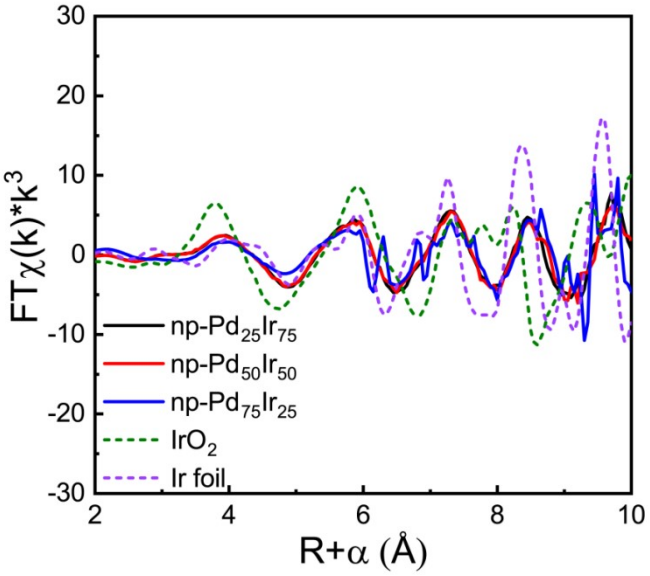

Figure S6. *k* space oscillation mode of the EXAFS spectra for Ir L_3-edge.

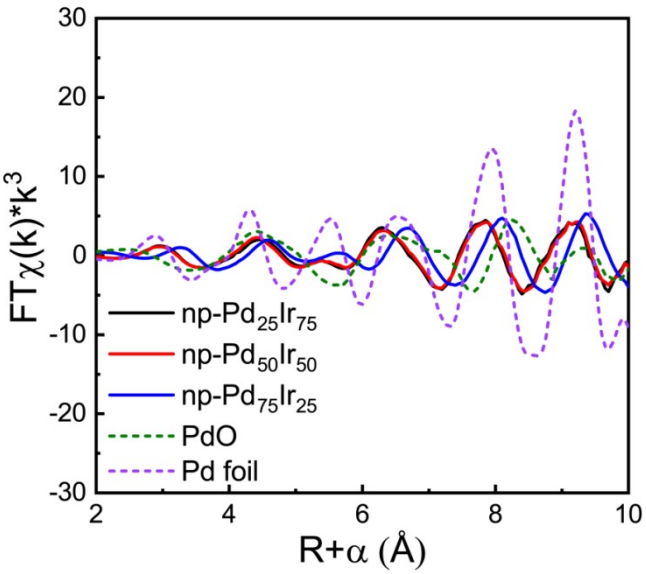

Figure S7. *k* space oscillation mode of the EXAFS spectra for Pd *K*-edge.

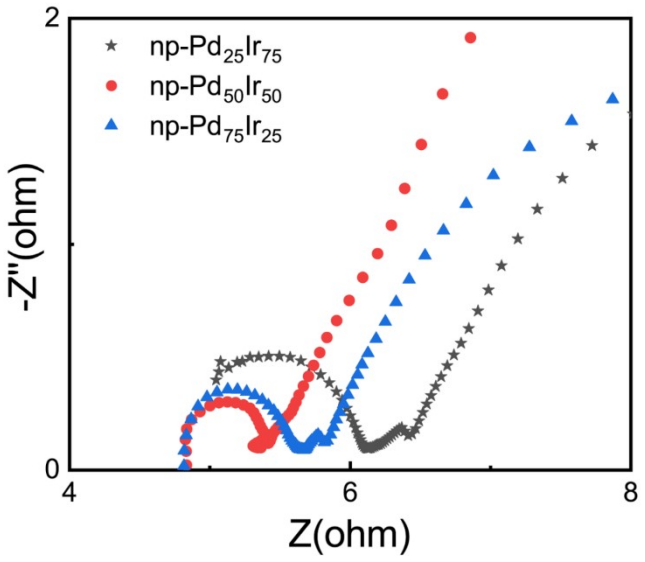

Figure S8. Electrochemical impedance spectroscopy measurements of np-$Pd_{100-x}Ir_x$ at 1.5 V versus RHE in 0.5 M H_2SO_4.

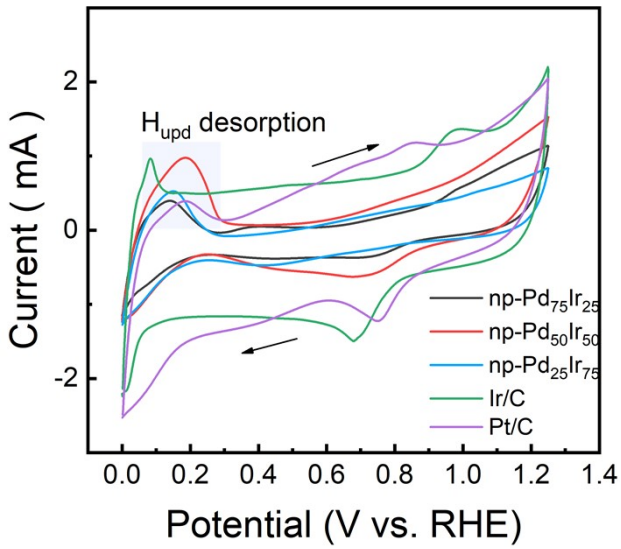

Figure S9. CV curves of np-$Pd_{75}Ir_{25}$, np-$Pd_{50}Ir_{50}$, np-$Pd_{25}Ir_{75}$, Ir/C, and Pt/C in 0.5 M H_2SO_4 with the scan rate of 10 mV s^{-1}.

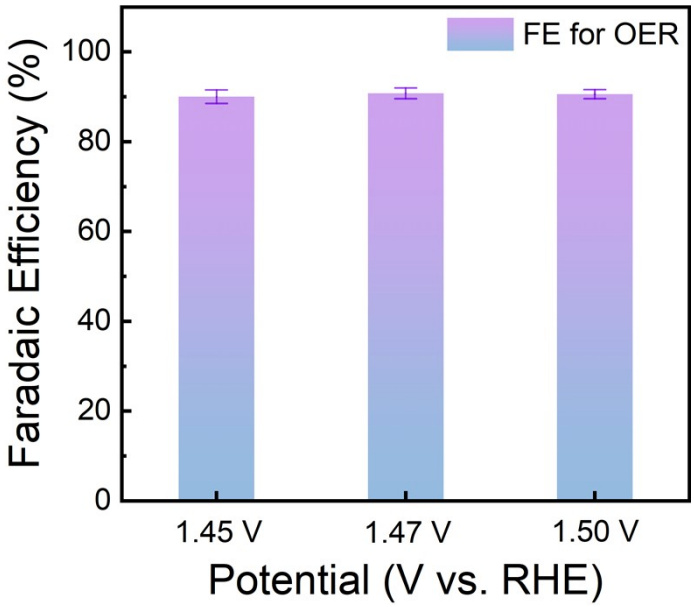

Figure S10. Faradaic efficiency of np-$Pd_{50}Ir_{50}$ for OER in 0.5 M H_2SO_4.

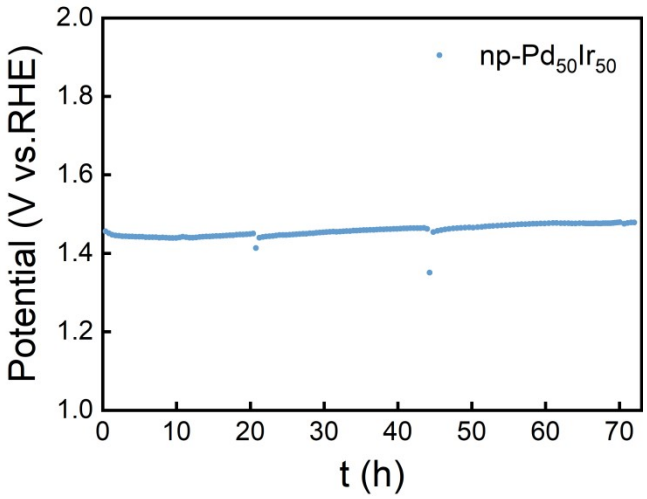

Figure S11. Chronopotentiometry curve of np-$Pd_{50}Ir_{50}$ for OER at 10 mA cm^{-2} in 0.5 M H_2SO_4.

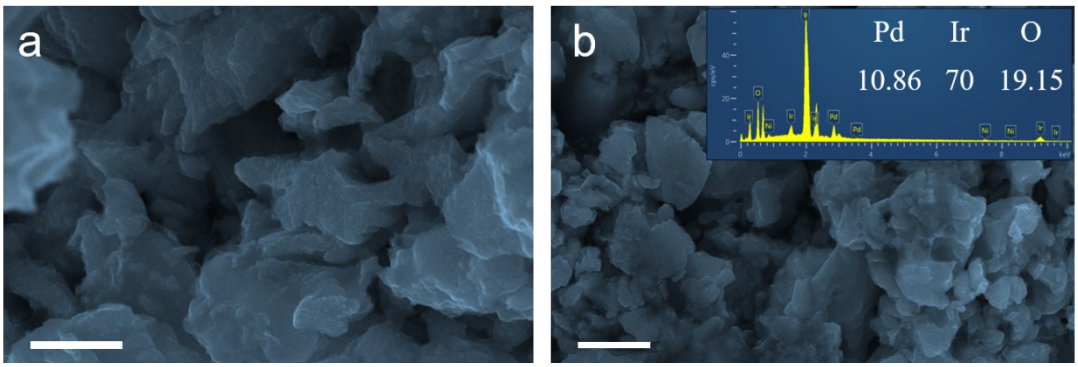

Figure S12. The SEM images of np-$Pd_{50}Ir_{50}$ after 72 hours OER test at 10 mA cm^{-2}. Scale bars: a) 1μm. b) 2μm.

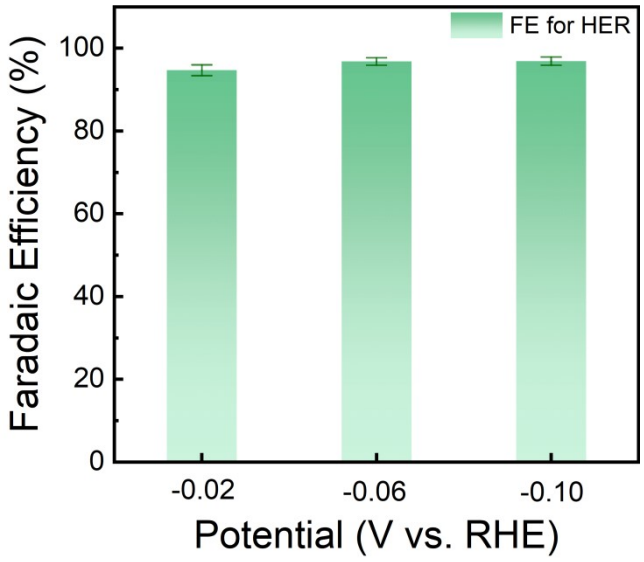

Figure S13. Faradaic efficiency of np-$Pd_{50}Ir_{50}$ for HER in 0.5 M H_2SO_4.

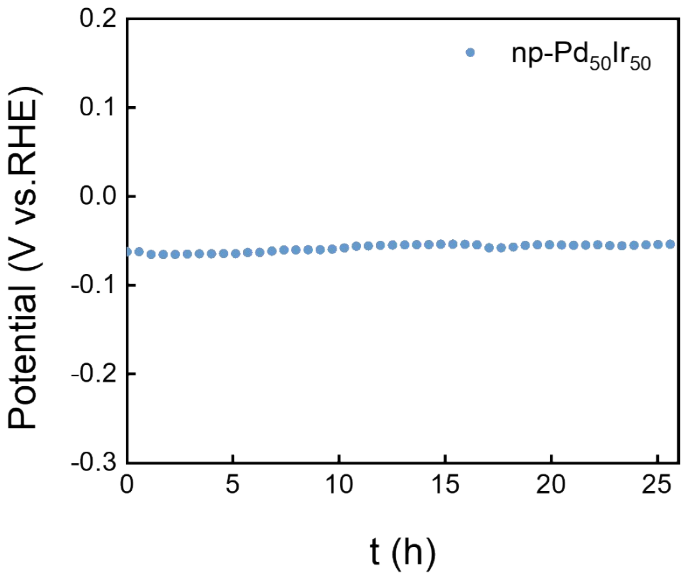

Figure S14. Chronopotentiometry curve of np-$Pd_{50}Ir_{50}$ for HER at 10 mA cm^{-2} in 0.5 M H_2SO_4.

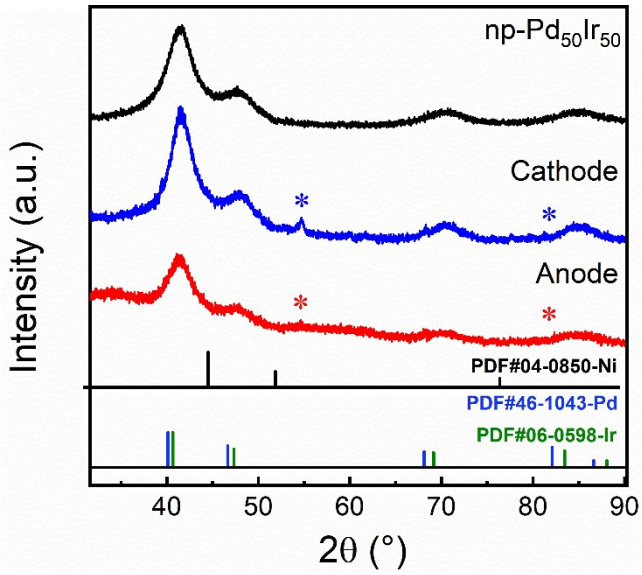

Figure S15. The XRD patterns of the catalysts after 25-h overall water splitting test in acidic electrolyte. *: The peak positions marked in the pattern are from C (PDF#26-1077), which is the result of carbon paper as the substrate interference.

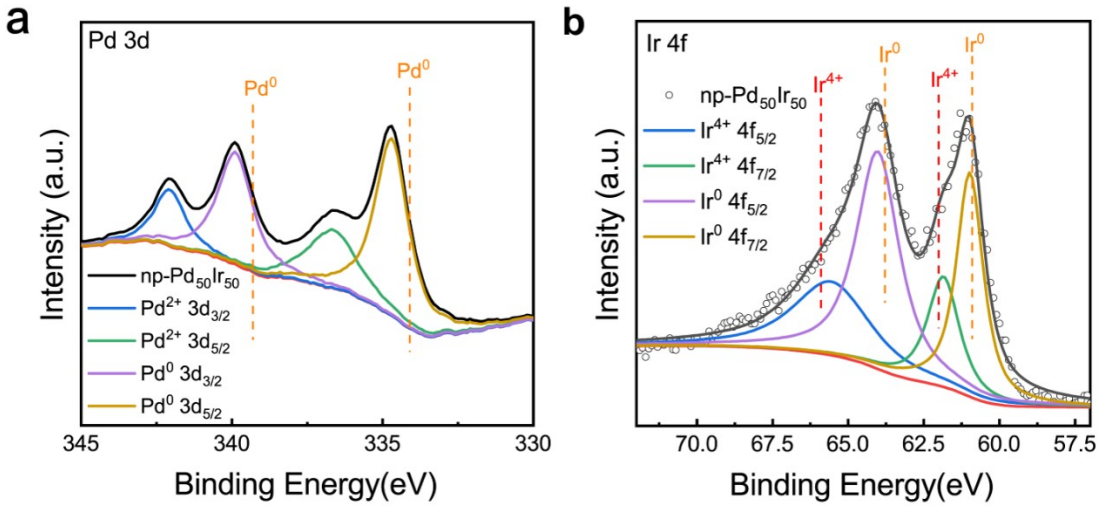

Figure S16. The XPS spectra of np-$Pd_{50}Ir_{50}$ after OER test for 25 h.

Pd 3d region **a)** and Ir 4f region **b)**. In Pd 3d region, the $3d_{3/2}$and $3d_{5/2}$ orbits were split into two peaks respectively, indicating the oxidation of Pd during the OER testing. In Ir 4f region, the $4f_{7/2}$ and $4f_{5/2}$ peaks which located at 61.04 eV and 64.10 eV were split into two peaks respectively, indicating the oxidation of Ir in np-$Pd_{50}Ir_{50}$.[15]

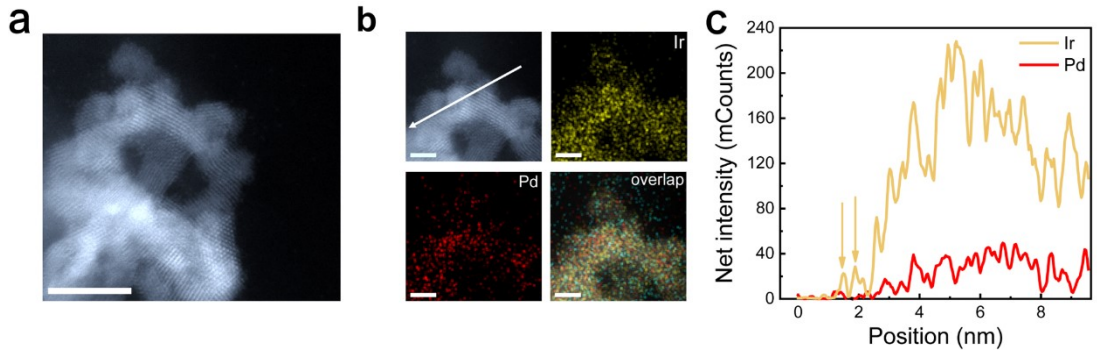

Figure S17. STEM characterizations of the anode catalyst (np-$Pd_{50}Ir_{50}$) after long-time operation in acidic solution.

a) HAADF-STEM image of np-$Pd_{50}Ir_{50}$. **b)** The EDS elemental mapping. **c)** The linear scan of Ir and Pd elements pattern along the path of the white arrow in **b)**. Scale bars: **a)** 5 nm. **b)** 2 nm.

Table S1. Comparison of the ECSA for the prepared electrocatalysts, commercial Ir/C and Pd/C calculated by H_{UPD} method.

Catalysts	ECSA (m^2 $g_{Ir+Pd\ or\ Pt}^{-1}$)
np-$Pd_{25}Ir_{75}$	65.67
np-$Pd_{50}Ir_{50}$	137.61
np-$Pd_{75}Ir_{25}$	51.03
Ir/C	70.62
Pt/C	91.24

Table S2. Comparison of the OER mass activity and specific activity for the prepared electrocatalysts and commercial Ir/C at an overpotential of 270 mV.

Catalysts	Mass activity ($A\ mg_{Ir}^{-1}$)	Mass activity ($A\ mg_{Ir+Pd}^{-1}$)	Specific activity ($A\ m^{-2}$)
np-$Pd_{25}Ir_{75}$	0.72	0.58	8.75
np-$Pd_{50}Ir_{50}$	3.80	2.50	18.17
np-$Pd_{75}Ir_{25}$	0.99	0.43	8.33
Ir/C	0.34	-	4.74

Table S3. OER performances of np-$Pd_{50}Ir_{50}$ and other reported electrocatalysts in acidic electrolyte.

Catalysts	Electrolytes	Overpotential (mV) at 10 mA cm^{-2}	Tafel slope (mV dec^{-1})	Ref.
np-$Pd_{50}Ir_{50}$	0.5 M H_2SO_4	217	58.0	This work
Ir-Pd nanowires	0.5 M H_2SO_4	300	60.0	16
$Pd@Ir_{3L}$	0.1 M H_2SO_4	263	59.3	17
Pt-Ir-Pd	0.1 M $HClO_4$	408	128.7	18
IrCo@NCNT/PC	0.5 M H_2SO_4	300	56.0	19
RuIr@CoNC	0.5 M H_2SO_4	223	45.0	20
Ir p-NHs	0.5 M H_2SO_4	243	51.0	21
Co-RuIr	0.1 M $HClO_4$	235	66.9	22
IrTe nanotubes	0.1 M $HClO_4$	290	60.3	23
$Au@AuIr_2$	0.5 M H_2SO_4	261	58.3	24
$Ir_{0.5}Ru_{0.5}$	0.5 M H_2SO_4	219	60.7	25
Ir_xPd MNNS	0.5 M H_2SO_4	307	65.7	26
$Ir_{0.5}W$	0.1 M	290	42.0	27

	$HClO_4$			
Ir/FeN_4	0.5 M H_2SO_4	316	61.5	28
IrRu@Te	0.5 M H_2SO_4	220	35.0	29
$Cr_{0.6}Ru_{0.4}O_2$	0.5 M H_2SO_4	178	48.0	30
$Li\text{-}IrO_2$	0.5 M H_2SO_4	270	39.0	31
IrCuNi	0.1 M $HClO_4$	273	41.0	32

Table S4. HER performances of np-$Pd_{50}Ir_{50}$ and other reported electrocatalysts in acidic electrolyte.

Catalysts	Electrolytes	Overpotential (mV) at 10 mA cm^{-2}	Tafel slope (mV dec^{-1})	Ref.
np-$Pd_{50}Ir_{50}$	0.5 M H_2SO_4	20.00	24.0	This work
Pt_3Co@NCNT	0.5 M H_2SO_4	42.00	27.2	33
Pt@Co SAs-ZIF-NC	0.5 M H_2SO_4	27.00	21.0	34
$PdCu_{0.2}H_{0.43}$	0.5 M H_2SO_4	28.00	23.0	35

Ni/np-Ir	0.5 M H_2SO_4	17.00	24.0	1
Ir-Co-W NPs	0.5 M H_2SO_4	35.82	38.4	36
Ir-SA@Fe@NCNT	0.5 M H_2SO_4	26.00	31.8	37
$Pd_{13}Cu_3S_7$ NPs	0.5 M H_2SO_4	64.00	49.6	38
Au@PdAg NRBs	0.5 M H_2SO_4	26.20	30.0	39
α-$Ni(OH)_2$@Ir	0.5 M H_2SO_4	20.00	12.5	40
$Ir_{0.5}Ru_{0.5}$ nanocages	0.5 M H_2SO_4	18.00	25.0	25
Co-RuIr	0.1 M $HClO_4$	41.00	31.1	22
RuIr-NC	0.1 M $HClO_4$	42.00	38.3	41
IrRu NPs	0.5 M H_2SO_4	52.00	36.2	42
IrNi NCs	0.5 M H_2SO_4	19.00	33.5	43

Table S5. Comparison of the HER mass activity and specific activity for the prepared electrocatalysts, commercial Ir/C and Pt/C at an overpotential of 70 mV.

Catalysts	Mass activity ($A\ mg_{Ir+Pd\ or\ Pt}^{-1}$)	Specific activity ($A\ m^{-2}$)
np-$Pd_{25}Ir_{75}$	0.25	3.81
np-$Pd_{50}Ir_{50}$	2.55	18.50
np-$Pd_{75}Ir_{25}$	0.34	6.57
Ir/C	1.04	14.73
Pt/C	2.10	23.06

Table S6. Overall water splitting performances of np-$Pd_{50}Ir_{50}$ and other reported electrocatalysts in acidic electrolyte.

Catalysts	Electrolytes	Potential (V) at 10 $mA\ cm^{-2}$	Ref.
np-$Pd_{50}Ir_{50}$	0.5 M H_2SO_4	1.52	This work
Pt/C//Ir/C	0.5 M H_2SO_4	1.60	This work
RuO_2-WC NPs	0.5 M H_2SO_4	1.66	44
Ir/g-C_3N_4/NG	0.5 M H_2SO_4	1.56	45
RuIr	0.1 M $HClO_4$	1.52	46
PdCu/Ir	0.5 M H_2SO_4	1.58	47
$Pt_{0.15}Pd_{0.30}Ru_{0.30}Cu_{0.25}$	0.5 M H_2SO_4	1.56	48

Ir-GF	0.5 M H_2SO_4	1.55	49
IrNi NCs	0.5 M H_2SO_4	1.58	50
Ir p-NH	0.5 M H_2SO_4	1.50	21
AuIr@CNT	0.5 M H_2SO_4	1.51	40
Ir-Ag nanotubes	0.5 M H_2SO_4	1.55	51
Ir-WO_3	0.5 M H_2SO_4	1.56	52
$IrCo_{0.65}$	0.1 M $HClO_4$	1.59	53

References

[1] Y. Q. Yu, K. Jiang, M. Luo, Y. Zhao, J. Lan, M. Peng, F. M. F. de Groot and Y. W. Tan, *ACS Nano*, 2021, **15**, 5333-5340.

[2] M. B. Stevens, L. J. Enman, A. S. Batchellor, M. R. Cosby, A. E. Vise, C. D. M. Trang and S. W. Boettcher, *Chem. Mater.*, 2017, **29**, 120-140.

[3] T. Y. Ma, S. Dai, M. Jaroniec and S. Z. Qiao, *J. Am. Chem. Soc.*, 2014, **136**, 13925-13931.

[4] J. W. Nai, Y. Lu, L. Yu, X. Wang and X. W. Lou, *Adv. Mater.*, 2017, **29**, 1703870.

[5] M. Chauhan, K. P. Reddy, C. S. Gopinath and S. Deka, *ACS Catal.*, 2017, **7**, 5871-5879.

[6] K. Jiang, B. Liu, M. Luo, S. Ning, M. Peng, Y. Zhao, Y. R. Lu, T. S. Chan, F. M. F. De Groot and Y. Tan, *Nat. Commun.*, 2019, **10**, 1743.

[7] P. A. Kempler and A. C. Nielander, *Nat. Commun.*, 2023, **14**, 1158-1158.

[8] Q. Dang, H. Lin, Z. Fan, L. Ma, Q. Shao, Y. Ji, F. Zheng, S. Geng, S.-Z. Yang, N. Kong, W. Zhu, Y. Li, F. Liao, X. Huang and M. Shao, *Nat. Commun.*, 2021, **12**, 6007.

[9] W. Li and A. M. Lane, *Electrochem. Commun.*, 2011, **13**, 913-916.

[10] P.-C. Chen, M. Li, J. Jin, S. Yu, S. Chen, C. Chen, M. Salmeron and P. Yang, *ACS Mater. Lett.*, 2021, **3**, 1440-1447.

[11] H. Wang, J. Qi, N. Yang, W. Cui, J. Wang, Q. Li, Q. Zhang, X. Yu, L. Gu, J. Li, R. Yu, K. Huang, S. Song, S. Feng and D. Wang, *Angew. Chem. Int. Ed.*, 2020, **59**, 19691-19695.

[12] J. Kibsgaard, C. Tsai, K. Chan, J. D. Benck, J. K. Nørskov, F. Abild-Pedersen and T. F. Jaramillo, *Energy Environ. Sci.*, 2015, **8**, 3022-3029.

[13] T. T. Liu, W. B. Gao, Q. Q. Wang, M. L. Dou, Z. P. Zhang and F. Wang, *Angew. Chem. Int. Ed.*, 2020, **59**, 20423-20427.

[14] W. C. Xu, G. L. Fan, J. L. Chen, J. H. Li, L. Zhang, S. L. Zhu, X. C. Su, F. Y. Cheng and J. Chen, *Angew. Chem. Int. Ed.*, 2020, **59**, 3511-3516.

[15] Y. K. Zhang, C. Q. Wu, H. L. Jiang, Y. X. Lin, H. J. Liu, Q. He, S. M. Chen, T. Duan and L. Song, *Adv. Mater.*, 2018, **30**, 1707522.

[16] T. Zhang, S. A. Liao, L. X. Dai, J. W. Yu, W. Zhu and Y. W. Zhang, *Sci. China Mater.*, 2018, **61**, 926-938.

[17] J. W. Zhu, Z. H. Lyu, Z. T. Chen, M. H. Xie, M. F. Chi, W. Q. Jin and Y. N. Xia, *Chem. Mater.*, 2019, **31**, 5867-5875.

[18] J. W. Zhu, M. H. Xie, Z. T. Chen, Z. H. Lyu, M. F. Chi, W. Q. Jin and Y. N. Xia, *Adv. Energy Mater.*, 2020, **10**, 1904114.

[19] D. K. Zhao, Y. G. Zhu, Q. K. Wu, W. Zhou, J. C. Dan, H. Zhu, W. Lei, L. J. Ma and L. G. Li, *Chem. Eng. J.*, 2022, **430**, 132825.

[20] J. Y. Xu, J. J. Li, Z. Lian, A. Araujo, Y. Li, B. Wei, Z. P. Yu, O. Bondarchuk, I. Amorim, V. Tileli, B. Li and L. F. Liu, *ACS Catal.*, 2021, **11**, 3402-3413.

[21] X. B. Bao, S. J. Li, C. T. Hao, Y. F. Qin, Y. T. Gong, Y. Yang, A. N. Xu and M. C. Luo, *J. Mater. Chem. A*, 2022, **10**, 20005-20010.

[22] J. Q. Shan, T. Ling, K. Davey, Y. Zheng and S. Z. Qiao, *Adv. Mater.*, 2019, **31**, 1900510.
[23] Q. R. Shi, C. Z. Zhu, D. Du, J. Wang, H. B. Xia, M. H. Engelhard, S. Feng and Y. H. Lin, *J. Mater. Chem. A*, 2018, **6**, 8855-8859.
[24] H. M. Wang, Z. N. Chen, D. S. Wu, M. N. Cao, F. F. Sun, H. Zhang, H. H. You, W. Zhuang and R. Cao, *J. Am. Chem. Soc.*, 2021, **143**, 4639-4645.
[25] S. Z. Wang, S. Yang, Z. Q. Wei, Y. J. Liang, J. W. Zhu, Y. W. Tang and X. Y. Qiu, *J. Mater. Chem. A*, 2022, **10**, 25556-25563.
[26] H. Y. Tian, W. L. Zhu, Q. R. Shi, S. C. Ding, Z. Y. Lyu, M. J. Xu, X. Q. Pan, M. H. Engelhard, D. Dan and Y. H. Lin, *J. Mater. Chem. A*, 2022, **10**, 11196-11204.
[27] J. J. Gao, X. Huang, W. Z. Cai, Q. L. Wang, C. M. Jia and B. Liu, *ACS Appl. Mater. Interfaces*, 2020, **12**, 25991-26001.
[28] B. M. Tackett, W. C. Sheng, S. Kattel, S. Y. Yao, B. H. Yan, K. A. Kuttiyiel, Q. Y. Wu and J. G. G. Chen, *ACS Catal.*, 2018, **8**, 2615.
[29] J. Y. Xu, Z. Lian, B. Wei, Y. Li, O. Bondarchuk, N. Zhang, Z. P. Yu, A. Araujo, I. Amorim, Z. C. Wang, B. Li and L. F. Liu, *ACS Catal.*, 2020, **10**, 3571-3579.
[30] Y. C. Lin, Z. Q. Tian, L. J. Zhang, J. Y. Ma, Z. Jiang, B. J. Deibert, R. X. Ge and L. Chen, *Nat. Commun.*, 2019, **10**, 162.
[31] J. J. Gao, C. Q. Xu, S. F. Hung, W. Liu, W. Z. Cai, Z. P. Zeng, C. M. Jia, H. M. Chen, H. Xiao, J. Li, Y. Q. Huang and B. Liu, *J. Am. Chem. Soc.*, 2019, **141**, 3014-3023.
[32] D. Liu, Q. Q. Lv, S. Q. Lu, J. J. Fang, Y. F. Zhang, X. D. Wang, Y. R. Xue, W. Zhu and Z. B. Zhuang, *Nano Lett.*, 2021, **21**, 2809-2816.
[33] S. L. Zhang, X. F. Lu, Z. P. Wu, D. Y. Luan and X. W. Lou, *Angew. Chem. Int. Ed.*, 2021, **60**, 19068-19073.
[34] L. H. Liang, H. H. Jin, H. Zhou, B. S. Liu, C. X. Hu, D. Chen, Z. Wang, Z. Y. Hu, Y. F. Zhao, H. W. Li, D. P. He and S. C. Mu, *Nano Energy*, 2021, **88**, 106221.
[35] Y. Y. Jia, T. H. Huang, S. Lin, L. S. Guo, Y. M. Yu, J. H. Wang, K. W. Wang and S. Dai, *Nano Lett.*, 2022, **22**, 1391-1397.
[36] M. Kim, H. Kang, E. Hwang, Y. Park, W. Jeong, Y. J. Hwang and D. H. Ha, *Appl. Surf. Sci.*, 2023, **612**, 155862.
[37] F. Luo, H. Hu, X. Zhao, Z. H. Yang, Q. Zhang, J. X. Xu, T. Kaneko, Y. Yoshida, C. Z. Zhu and W. W. Cai, *Nano Lett.*, 2020, **20**, 2120-2128.
[38] J. Park, H. Jin, J. Lee, A. Oh, B. Kim, J. H. Kim, H. Baik, S. H. Joo and K. Lee, *Chem. Mater.*, 2018, **30**, 6884-6892.
[39] Z. X. Fan, Z. M. Luo, X. Huang, B. Li, Y. Chen, J. Wang, Y. L. Hu and H. Zhang, *J. Am. Chem. Soc.*, 2016, **138**, 1414-1419.
[40] Y. H. Xie, X. X. Yu, X. W. Li, X. Long, C. F. Chang and Z. H. Yang, *Chem. Eng. J.*, 2021, **424**, 130337.
[41] D. S. Wu, K. Kusada, S. Yoshioka, T. Yamamoto, T. Toriyama, S. Matsumura, Y. N. Chen, O. Seo, J. Kim, C. Song, S. Hiroi, O. Sakata, T. Ina, S.

Kawaguchi, Y. Kubota, H. Kobayashi and H. Kitagawa, *Nat. Commun.*, 2021, **12**, 1145.
[42] J. Joo, H. Jin, A. Oh, B. Kim, J. Lee, H. Baik, S. H. Joo and K. Lee, *J. Mater. Chem. A*, 2018, **6**, 16130-16138.
[43] Y. C. Pi, Q. Shao, P. T. Wang, J. Guo and X. Q. Huang, *Adv Funct Mater*, 2017, **27**, 1700886.
[44] S. C. Sun, H. Jiang, Z. Y. Chen, Q. Chen, M. Y. Ma, L. Zhen, B. Song and C. Y. Xu, *Angew. Chem. Int. Ed.*, 2022, **61**, e202202519.
[45] B. Jiang, T. Wang, Y. Cheng, F. Liao, K. Wu and M. Shao, *ACS Appl. Mater. Interfaces*, 2018, **10**, 39161-39167.
[46] J. Shan, T. Ling, K. Davey, Y. Zheng and S. Z. Qiao, *Adv. Mater.*, 2019, **31**, 1900510.
[47] M. Li, Z. Zhao, Z. Xia, M. Luo, Q. Zhang, Y. Qin, L. Tao, K. Yin, Y. Chao, L. Gu, W. Yang, Y. Yu, G. Lu and S. Guo, *Angew. Chem. Int. Ed.*, 2021, **60**, 8243-8250.
[48] M. Kim, Y. Kim, M. Y. Ha, E. Shin, S. J. Kwak, M. Park, I. D. Kim, W. B. Jung, W. B. Lee, Y. Kim and H. T. Jung, *Adv. Mater.*, 2023, DOI: 10.1002/adma.202211497.
[49] J. Zhang, G. Wang, Z. Q. Liao, P. P. Zhang, F. X. Wang, X. D. Zhuang, E. Zschech and X. L. Feng, *Nano Energy*, 2017, **40**, 27-33.
[50] Y. Pi, Q. Shao, P. Wang, J. Guo and X. Huang, *Adv Funct Mater*, 2017, **27**, 1700886.
[51] M. Zhu, Q. Shao, Y. Qian and X. Huang, *Nano Energy*, 2019, **56**, 330-337.
[52] P. Li, X. Duan, Y. Kuang and X. Sun, *Small*, 2021, **17**, 2102078.
[53] L. Fu, X. Zeng, G. Cheng and W. Luo, *ACS Appl. Mater. Interfaces*, 2018, **10**, 24993-24998.